Crystal structures in binary hard-sphere colloid-droplet mixtures with patchy cross interactions

Hai Pham Van [1,2] Andrea Fortini,[3] and Matthias Schmidt [1,*]

[1]*Theoretische Physik II, Physikalisches Institut, Universität Bayreuth, Universitätsstraße 30, D-95440 Bayreuth, Germany*

[2]*Department of Physics, Hanoi National University of Education, 136 Xuanthuy, Hanoi, Vietnam*

[3]*Department of Physics, University of Surrey, Guildford GU2 7XH, United Kingdom*

(Received 28 April 2017; published 27 January 2020)

A binary mixture of droplets and patchy colloids, where patches are arranged in tetrahedral symmetry, is studied with Metropolis Monte Carlo simulations. The colloidal patches attract droplets, while both the colloid-colloid and the droplet-droplet interactions are hard sphere like. We find stable crystal structures with atomic analogs ZnS, CaF_2, and fcc or hcp (face centered cubic or hexagonal close packed) of the droplets coexisting with a dispersed fluid of the colloids. The simulated crystal structures agree well with those predicted by close-packing calculations for an intermediate range of droplet-colloid size ratios. A discrepancy between the simulations and theoretical predictions occurs at low and high size ratios. The results of the simulations for mixtures with anisotropic colloid-droplet interactions reveal a richer phase diagram, with ZnS-gas and ZnS-fluid coexistence, as compared to the isotropic case. For the example of a square planar patch arrangement, we find a particular crystal structure, consisting of two interpenetrating fcc or hcp lattices with right bond angles. Such a structure has no known atomic analog. Our study of generic models of anisotropic colloid-droplet mixtures could provide a promising way towards the fabrication of novel and complex colloidal structures.

DOI: 10.1103/PhysRevE.101.012608

I. INTRODUCTION

The designed self-assembly of colloidal particles is a topic of strong current interest [1]. In particular, creating colloidal crystal structures has attracted much attention due to the potential applications as chemical sensors [2], as well as macroporous [3] and photonic materials [4,5]. Among the lattice structures with three-dimensional (3D) complete photonic band gaps in the visible light region, the diamond lattice is one of the most promising candidates [6,7].

To date, however, such a structure has not been experimentally fabricated despite recent advances in the fabrication of complex colloidal particles with chemically or physically patterned surfaces [8–14], as well as a large number of theoretical suggestions for its colloidal self-assembly. For example, Tkachenko [15] first reported that the diamond lattice can be achieved by self-organization of DNA-covered colloids. The key element of that scheme is that the colloidal spheres are covered with short single-stranded DNA molecules, which induce a type-dependent interaction between colloids. These interactions are selective, reversible, and tunable. Furthermore, the formation of the diamond structure has been observed in computer simulations of colloids whose surfaces are decorated with attractive patches that are distributed in tetrahedral symmetry [16]. The formation of the diamond structure, however, requires systems with a seed crystal or a complicated directional-dependent pair potential [16]. Since then, the very rich phase diagram of tetrahedral patchy particles has been extensively investigated [17–23]. Unfortunately, it was found that the diamond phase only occurs in a very narrow range of densities [19,23]. Additionally, at low pressures and finite temperatures, the diamond is energetically comparable to a bcc solid. The diamond structure is only stable when the entropy increases, that is, when the interaction range decreases. As the pressure increases, the bcc solid becomes favored [19]. Doye *et al.* [24] also pointed out that the crystallization of single-component tetrahedral patchy colloids could be frustrated by the variety of local structures that are possible in the liquid phase.

An alternative strategy is based on the use of binary mixtures [25]. de las Heras *et al.* [26,27] investigated the gel structures and percolation in a binary mixture of patchy colloids, but these authors did not investigate crystal formation. The phase behavior and the structure of binary colloidal crystals are controlled by the size ratio of the two components, the total packing fraction, and the relative composition. It was found theoretically [28] and experimentally [29–31] that a change in the diameter ratio between the two spherical species has a dramatic effect on the phase diagram and produces a variety of different crystal structures with symmetry of NaCl, AlB_2, and $NaZn_{13}$, as well as Laves phases. Using a genetic algorithm and the principle of maximization of the packing density, Filion and Dijkstra [32] predicted additional crystal structures at infinite pressure, such as $HgBr_2$ and $AuTe_2$. Hopkins *et al.* [33,34] later investigated the densest packing of binary hard-sphere mixtures and predicted a large number of crystal structures with uncommon stoichiometries, including LS_6, LS_{10}, LS_{11}, L_2S_4, L_3S_7, and L_6S_6, of the large (L) and small (S) spheres. Cottin and Monson [35] examined other crystal structures with symmetry of ZnS and CaF_2, and found that in the cell theory approach, these structures would not be stable. ZnS can be generated by repeating the fcc or hcp unit cell of either species and filling half of the tetrahedral holes

*matthias.schmidt@uni-bayreuth.de

with the other species, namely, zinc blende or wurtzite. When the two species in the zinc blende are identical, the diamond structure is obtained. The structure of CaF_2 is similar to that of the zinc blende, but all of the tetrahedral holes are occupied. In particular, both the structures of ZnS and CaF_2 have been recently predicted to display 3D complete band gaps [36].

In this paper, we investigate the structural behavior of a binary mixture of hard-sphere colloids and emulsion droplets. The colloid-droplet interaction is aimed at modeling the Pickering effect modulated by a directional-dependent factor. This model, as a colloidal version of the methane molecule CH_4, is a straightforward extension of the system with an isotropic interaction studied by Fortini [37]. In the model, first proposed by Román *et al.* [38], the colloidal particles are able to penetrate the droplets. Fortini [37] and Schmidt and co-workers [39–41] used a similar model to investigate the cluster formation of spherical colloids, single-patch colloid, or dumbbell-shaped colloids and reported good agreement with experimental findings. However, the authors modeled and simulated the colloid-droplet mixtures with isotropic interactions. Here, we investigate a directionally dependent interaction given by tetrahedral patches on the colloidal particles. The droplets can only attach to the patches and not to the other areas on the surface of the particles. For example, the model could be realized by patches of different hydrophilicity than the rest of the colloidal surface. By calculating the packing fraction and total energy as a function of size ratios for the candidate crystal structures with tetrahedral bonds, we make predictions for the stability of different crystal structures at infinite pressures. The result from these predictions shows good agreement with simulation data for a certain broad range of size ratio. In particular, we find that stable structures of ZnS and CaF_2, which are promising as photonic crystals [36], are possible.

This paper is organized as follows. In Sec. II, we describe the model and methods. In Sec. III, we give the results for mixtures with tetrahedral patches and compare theoretical and simulation results. In Sec. IV, we briefly discuss other patch arrangements. In Sec. V, we draw our conclusions. A detail description of bond order parameters used and close-packing calculations are given in Appendices A and B, respectively.

II. MODEL AND METHODS

We consider a mixture of N_c patchy colloidal particles of diameter σ_c and N_d droplets of diameter σ_d. The droplets are attracted to the patches, but not to the rest of the colloidal surface. The colloid-colloid and droplet-droplet intraspecies pair interactions are taken to be hard-sphere potentials,

$$\phi_{ii}(r) = \begin{cases} \infty, & r < \sigma_i \\ 0 & \text{otherwise,} \end{cases} \tag{1}$$

between particles of the same species $i = c$ (colloid) or $i = d$ (droplet).

The patchy colloid-droplet pair interaction does not contain a hard core, but rather models the Pickering effect [42] of solid particles adsorbed at a fluid interface. The interaction potential is defined as

$$\phi_{cd}\left(\mathbf{r}_{ij}, \alpha_{ijk_{\min}}\right) = u_{\mathrm{PW}}(r_{ij}) f\left(\mathbf{r}_{ij}, \alpha_{ijk_{\min}}\right), \tag{2}$$

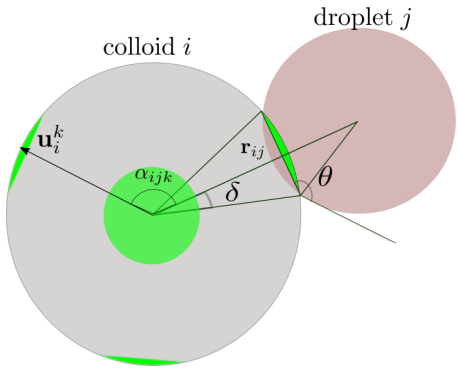

FIG. 1. Illustration of one tetrahedral patchy colloid and one droplet. Colloid i (gray sphere) has four patches (green parts) determined by a set of unit vectors $\{\mathbf{u}_i^k\}$ ($k = 1$–4) and patch size of half-opening angle δ. Droplet j (pink sphere) is located at the colloid surface. α_{ijk} is the angle formed between patch k on colloid i and the vector $\mathbf{r}_{ij}$ connecting the centers of colloid i and droplet j, and $k_{\min}$ is the patch that minimizes the magnitude of this angle. The case shown is when $\alpha_{ijk_{\min}} = 0$, i.e., the patch $k_{\min}$ points along the direction of the vector $\mathbf{r}_{ij}$. The contact angle θ is used to control the distance between colloid i and droplet j.

where $\mathbf{r}_{ij}$ is the distance vector connecting the centers of colloid i and droplet j and $r_{ij} = |\mathbf{r}_{ij}|$; α_{ijk} is the angle between $\mathbf{r}_{ij}$ and the unit vector pointing from the center of colloid i towards its kth patch; $\alpha_{ijk_{\min}} = \min \alpha_{ijk}$ with $k = 1, 2, 3, 4$ (see Fig. 1); and $u_{\mathrm{PW}}(r_{ij})$ is an isotropic parabolic well (PW) of depth ϵ, as used in Ref. [37],

$$u_{\mathrm{PW}}(r) = \begin{cases} A(r-B)^2 + C, & r < \frac{\sigma_d+\sigma_c}{2} \\ 0 & \text{otherwise,} \end{cases} \tag{3}$$

with parameters A, B, and C given by

$$\begin{aligned} A &= \frac{-\epsilon + \sqrt{\epsilon^2 + r_0^2}}{2r_0^2}, \\ B &= \frac{\sigma_d + \sigma_c}{2} - r_0, \\ C &= \frac{\epsilon - \sqrt{\epsilon^2 + r_0^2}}{2}, \end{aligned} \tag{4}$$

where

$$r_0 = \frac{\sigma_d}{2}(1 + \cos\theta), \tag{5}$$

with θ being the contact angle between droplets and colloids. In practice, the r_0 parameter is used to control the contact angle between droplets and colloids.

The parabolic well $u_{\mathrm{PW}}(r)$ is modulated in Eq. (2) by the factor $f(\mathbf{r}_{ij}, \alpha_{ijk_{\min}})$, which is a Gaussian-like function depending on the alignment of patches with the distance vector $\mathbf{r}_{ij}$. This potential is quite similar to that used by Noya *et al.* [43] and given by

$$f\left(\mathbf{r}_{ij}, \alpha_{ijk_{\min}}\right) = \exp\left(-\frac{4\alpha_{ijk_{\min}}^2}{\delta^2}\right), \tag{6}$$

where δ is the half-opening angle, which determines the widths of the patches. Obviously, as $1/\delta \to 0$, the anisotropic

potential in Eq. (2) become isotropic, $f(\mathbf{r}_{ij}, \alpha_{ijk_{\min}}) = 1$. As shown in Fig. 1, the half-opening angle δ is related to the contact angle θ and the diameter ratio by

$$\sin\delta = \frac{\sigma_d}{\sigma_c}\sin\theta. \tag{7}$$

The surface coverage χ is defined as the the (relative) ratio of the attractive surface area and the total surface area, and therefore relates to the half opening angle δ and the number of patches n_p by

$$\chi = n_p \sin^2\left(\frac{\delta}{2}\right). \tag{8}$$

The total interacting energy U_{tot} is the sum of all colloid-colloid, droplet-droplet, and colloid-droplet pair interactions,

$$\frac{U_{\text{tot}}}{k_{\text{B}}T} = \sum_{i<j}^{N_c}\phi_{cc}(|\mathbf{r}_i - \mathbf{r}_j|) + \sum_{i<j}^{N_d}\phi_{dd}(|\mathbf{R}_i - \mathbf{R}_j|) + \sum_{i}^{N_c}\sum_{j}^{N_d}\phi_{cd}\left(|\mathbf{r}_i - \mathbf{R}_j|, \alpha_{ijk_{\min}}\right), \tag{9}$$

where k_B is the Boltzmann constant, T is the temperature, $\mathbf{r}_i$ is the center-of-mass position of colloid i, and $\mathbf{R}_j$ is the center-of-mass position of droplet j.

We carry out Metropolis Monte Carlo (MC) simulations in the canonical ensemble, with 10^7 MC cycles for equilibration and 10^5 MC cycles for data production. In each MC cycle, all particles are attempted to be moved once on average. The droplets can only move translationally, whereas the colloids can both translate and rotate with adjustable trial moves to achieve an acceptance probability of around 50%. The initial random configuration of nonoverlapping spherical particles is prepared in a cubic box with periodic boundary condition. The simulations are carried out for the total number of colloids and droplets in the range 500–1000, i.e., at different particle packing fractions. The depth of the parabolic well is set to 10 k_BT to ensure state points within the crystal phase region (see Fig. 2(b) of Ref. [37]). Such a strongly short-ranged attraction could lead a suppression of collective motion and hence produce unphysical dynamics. To overcome this limitation, many algorithms have been proposed by the use of collective moves of clusters such as the rejection-free geometric cluster [44] or "virtual-move" Monte Carlo scheme [45]. In this study, however, we employ a standard Monte Carlo simulation with sequential moves of single particles and neglect the collective motion of particles in the cluster. In order to check the validity of the method used, we compared the resulting phase diagram, i.e., energy versus droplet packing fraction, for an isotropic pair interaction from Brownian dynamics simulations [37] with that of the current standard Monte Carlo simulation and find good agreement in the timescales considered. To improve the statistical quality, each physical quantity is simulated in five independent runs and then averaged.

To analyze the local structure of a given particle in the computer simulations, we employ the averaged local bond order parameters proposed by Lechner and Dellago [46], which allows us to distinguish liquidlike, fcc-like, hcp-like, and bcc-like particles. For details of the averaged bond order parameters, see Appendix A.

One of the major theoretical goals in research of colloidal crystals is to predict which crystal structure will be formed if the components of the system and their interactions are given. One relevant approach in predicting crystal structures involves free-energy calculations of different structural proposals. From these results, one would select the structure with the lowest free energy as that one to occur in nature. An alternative way to predict crystal structures for hard-sphere(-like) systems is to deal with packing arguments. The fundamental reason for using packing arguments is that crystal structures with a higher closed-packed density permit a larger local free volume for each sphere, resulting in a higher translational entropy and therefore a lower free energy [32].

According to Villars *et al.* [47], there are 147 classical atomic structures adopted by roughly 5000 binary compounds. This large number of structures results from a combination of composition, crystal system (unit-cell dimensions), space group, and occupation number. Fortunately, if we restrict our considerations to a given coordination number of four (with regular tetrahedral symmetry), then a much smaller number of candidate crystal structures needs to be considered, i.e., ZnS (zinc blende), ZnS (wurtzite), NaTl (zintl phase), CaF_2 (flourite), O_2Si ($\beta-$cristobalite),[1] and Cu_2O (cuprite). We denote these crystal structures by D_nC_m where two sets of spheres (D,C) represent droplets and colloids, respectively; n, m are integer numbers.

We define the packing fraction η as the ratio of the volume occupied by the spheres to the total volume in which they are enclosed. Based on an approach proposed by Parthé [48] and Sanders *et al.* [29], we calculate the packing fraction η and total potential energy U_{tot} as a function of size ratio, $q = \sigma_d/\sigma_c$, for the above crystal structures; see Appendix B for details. In a set of crystal structures of interest, the structure which has the highest packing fraction and lowest energy at a specific value of q will more likely occur than any other structures.

III. RESULTS FOR TETRAHEDRAL PATCHES

Given the large parameter space that controls our model, we decided to compute the stable phases at infinite pressure to guide our simulation study. In order to do so, we need to calculate the close-packing curves and the total energy of the closed-packed structures.

A. Fixed contact angle $\theta = 140°$

Figure 2(a) shows close-packing curves for the various structural proposals at the contact angle $\theta = 140°$. Each structure is characterized by a unique close-packing curve, except that the ZnS-zinc-blende and the ZnS-wurtzite structure have the same one since they belong to the same homeotect structure [49], i.e., all of the different structure types have equal composition and the same kind of surroundings. The equations used are reported in Appendix B. The curves for ZnS [see Eqs. (B1), (B6), (B9)] and CaF_2 [Eqs. (B12), (B13),

[1]The chemical formula SiO_2 is reversed to be consistent with the interchanged role of the two species.

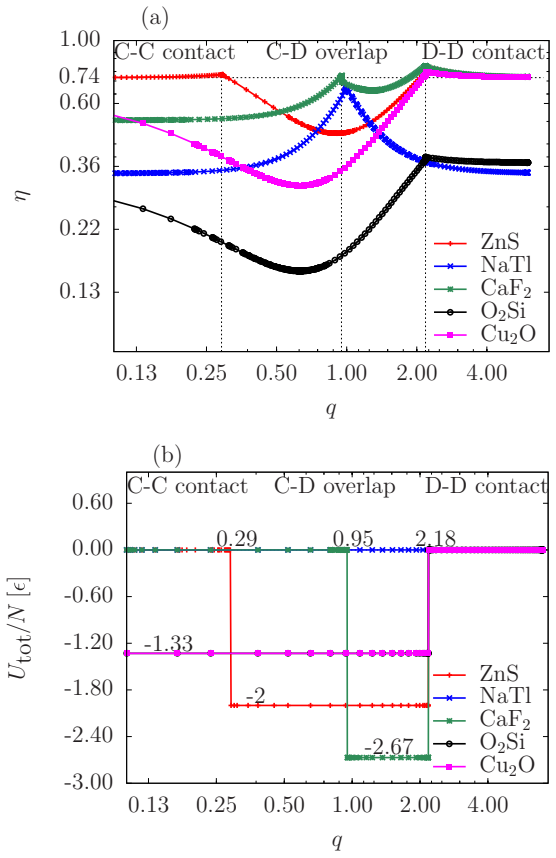

FIG. 2. (a) Close-packing curve as dependent upon the size ratio q for the ZnS, NaTl, CaF_2, O_2Si, and Cu_2O structure at $\theta = 140°$. A horizontal dashed line is added to indicate the maximum packing fraction (0.74) of a monodispersed system of hard spheres corresponding to fcc or hcp. (b) The scaled total energy per particle U_{tot}/N, with N the total number of particles, is plotted against q for different structures. Notice the logarithmic scales of η and q.

(B14)] show three distinct branches corresponding to C-C (colloid-colloid) contact, C-D (colloid-droplet) overlap, and D-D (droplet-droplet) contact regions. The NaTl structure has no C-D contact region, while O_2Si and Cu_2O have no C-C contact region.

Figure 2(b) shows the total energy per particle, U_{tot}/N, with $N = N_c + N_d$, as a function of the size ratio for the candidate structure types. From the total-energy curves and close-packing curves, we predict the phase diagram at infinite pressures because, for a given size ratio q, stable structures have the lowest energy and the largest packing fraction. We see from Figs. 2(a) and 2(b) that structural phase transitions occur at discontinuity points of the close-packing curves, i.e., at $q = 0.29$ (phase transition from Cu_2O to ZnS), $q = 0.95$ (ZnS-CaF_2), and $q = 2.18$ (CaF_2-fcc or -hcp of droplets with a dispersed fluid of colloids). Table I summarizes the stable structures at different size ratios q for the contact angle $\theta = 140°$.

To examine the stability of these crystal structures at finite pressures, we carry out MC simulations for different size ratios $q = 0.22$, 0.75, 0.97, and 1.5 at a fixed contact angle $\theta = 140°$. The total packing fraction and composition are predetermined according to each structure of interest. For

TABLE I. Structures predicted theoretically for different values of size ratios at infinite pressure and $\theta = 140°$.

Size ratio ($q = \frac{\sigma_d}{\sigma_c}$)	Structure type
$q < 0.29$	Cu_2O
$0.29 < q < 0.95$	ZnS
$0.95 < q < 2.18$	CaF_2
$q > 2.18$	fcc or hcp of droplets + fluid of colloids

$q = 0.22$, we find a homogenous fluid phase instead of the Cu_2O crystalline phase as predicted by theory. This result can be explained as follows. Since the attractive area fraction of colloids, which is related to the droplet ratio according to Eqs. (7) and (8), is relatively small, the probability of capturing the droplets at the colloid surface is low. Note also that the depth of the colloid-droplet interaction potential is still kept the same, while the width becomes significantly narrower. Therefore, the system behaves nearly as a highly asymmetric binary hard-sphere mixture, which was shown to be in the fluid phase at $q = 0.2$ [50] and at the packing fraction of particles equal to that in our simulations.

Figure 3 shows simulation snapshots for the size ratio $q = 0.75$. In Fig. 3(a), the large (yellow) spheres represent the colloids, while the small (green) spheres represent the droplets. It can be seen that the colloids and droplets assemble into a periodic three-dimensional lattice, where each colloid is surrounded by four droplets (green spheres) located at the attractive (blue) patches of this colloid. Figure 3(b) shows the snapshot of the same system, but each particle is colored corresponding to its state [46]. A coexistence phase of fcc and hcp for both the droplets and colloids can be observed, which results from a marginal difference in the free energy between two competing structures. In order to take further steps in potential applications, such as photonic band-gap materials that are required to stabilize a selected crystal polymorph from competing structures, i.e., removal of the hexagonal ordering of colloids or droplets from random stackings of fcc and hcp crystal, one could introduce polymers with appropriate geometries used as depletants into the void symmetries of the binary crystal phase. The introduction, as shown in recent studies by Mahynski and co-workers [51–54], produces a

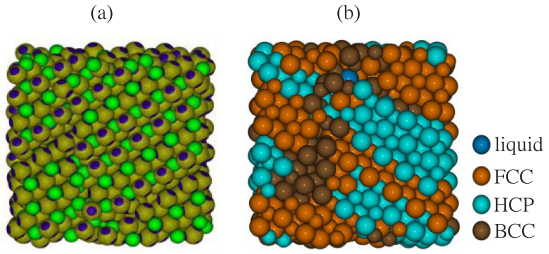

FIG. 3. (a) Snapshot of the colloid-droplet mixture in the final stage of the computer simulation at $q = 0.75$, $\eta_c = 0.348$, $\eta_d = 0.146$, $N_d/N_c = 1$. Large dark yellow spheres represent the colloids; smaller green spheres represent the droplets. Each colloid is decorated by four attractive patches (blue) on its surface. (b) Same as (a), but the state of each particle is identified by the local average bond order parameters.

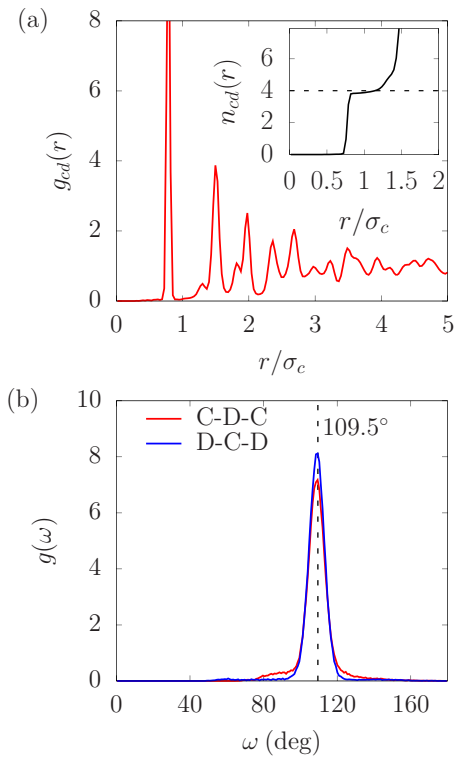

FIG. 4. (a) MC simulation results for the colloid-droplet radial distribution function $g_{cd}(r)$ as a function of the scaled distance r/σ_c. Inset: the number of droplets $n_{cd}(r)$ as a function of the distance r/σ_c from a reference colloid, which is determined by integration of $g_{cd}(r)$. (b) Angular distribution function $g(\omega)$ of colloid-droplet-colloid (C-D-C) and droplet-colloid-droplet (D-C-D) angles ω. The label 109.05° marks the bond angle of a regular tetrahedron.

significant entropy difference in the different polymorphs, and therefore provides a sufficient driving force to uniquely select a single polymorph. An alternative strategy proposed by Romano and Sciortino [55] is based on a rational design of patch shape and symmetry, called patterning symmetry, that also removes the structural polymorphism and the formation of random stacks of competing structures. The colloid-droplet radial distribution function given in Fig. 4(a) shows well-defined long-ranged peaks characteristic of a specific crystal phase. Furthermore, the coordination number as a function of the scaled distance [see the inset of Fig. 4(a)] and angular distribution functions [Fig. 4(b)] strongly confirm the existence of regular tetrahedral bonds of the droplets with the colloids. These results enable us to classify the phase of the colloid-droplet mixture at $q = 0.75$ as the ZnS crystal structure, which is in good accordance with the result predicted by the theory; cf. Table I.

For the case of $q = 0.97$, the total packing fraction for the perfect CaF_2 structure once formed ($\eta = 0.748$) is so high that an initialization from a random configuration of droplets and colloids could not be performed with our present algorithm, and hence we set the composition N_d/N_c to be the same as for the case of $q = 0.75$. As a result, when the CaF_2 structure is formed, it will have some missing bonds. Despite the lack of some bonds, the CaF_2 structure is still easily detected by analyzing angular distribution functions. As

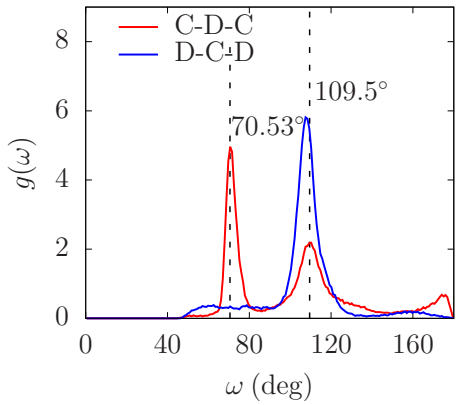

FIG. 5. Angular distribution functions for the colloid-droplet mixture at $q = 0.97$, $\eta_c = 0.257$, $\eta_d = 0.234$, and $N_d/N_c = 1$. The labels 70.53° and 109.05° indicate two pronounced peaks that are characteristic of the CaF_2 structure.

shown in Fig. 5, two pronounced peaks at 70.53° and 109.5° in the colloid-droplet-colloid angular distribution function and one peak at 109.5° in the droplet-colloid-droplet angular distribution function demonstrate the occurrence of the CaF_2 structure. This result again agrees well with the theoretical prediction. At a higher size ratio, e.g., $q = 1.5$, different from a binary crystal phase observed in the case of the isotropic colloid-droplet pair interaction [37] and from the CaF_2 phase for $q < 2.18$ given in Table I, we find a fcc or hcp phase of the droplets coexisting with a fluid of the colloids.

Stability of the ZnS structure with respect to anisotropy of the interaction

In order to investigate the equilibrium phases for the ZnS structure, which was shown to be a promising candidate for 3D complete photonic band-gap materials [36], we carry out simulations for each state point in the (η_d, η_c) plane, with η_d (η_c) the droplet (colloid) packing fraction for $q = 0.75$. At first, we consider two cases: isotropic [i.e., setting $f(\mathbf{r}_{ij}, \alpha_{ijk_{\min}}) = 1$ in Eq. (2)] and anisotropic colloid-droplet pair interaction (cf. Sec. II).

As shown in Figs. 6(a) and 6(b), for both cases, we find a region where the fluid is stable (marked by blue filled squares) and a region where gas-liquid separation occurs (orange circles). In addition to that, for the anisotropic colloid-droplet pair interaction, we find a region where the system separates into a gas and a ZnS crystal (empty squares) and another region where the system separates into a fluid and a ZnS crystal (red triangles).

B. Variation of the contact angle parameter

The variation of the contact angle θ changes the discontinuity points in the close-packing curves, leading to different transition regions for the crystalline structures. In Fig. 7, we map out the phase diagram in the $(\theta - q)$ representation. We also show the comparison between the phase diagram obtained from the theory (differently colored regions) and the simulation results (differently shaped symbols). We find that the simulated state points of ZnS and CaF_2 show good

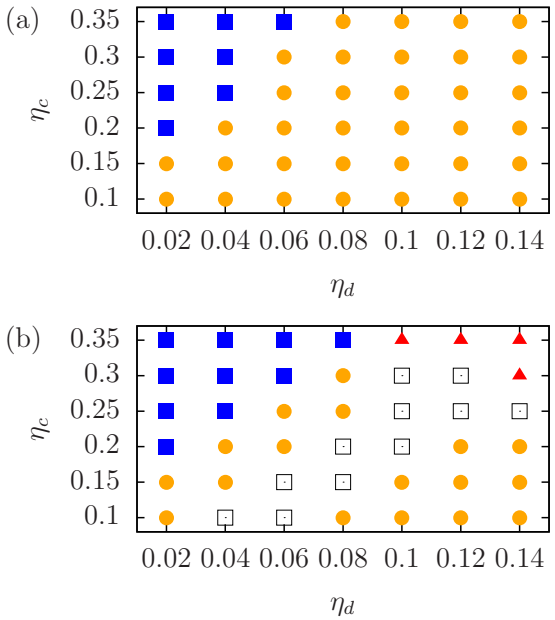

FIG. 6. (η_d, η_c) phase diagrams of the colloid-droplet binary mixture with the diameter ratio $q = 0.75$ and $\theta = 140^\circ$: (a) isotropic colloid-droplet pair potential, (b) anisotropic colloid-droplet pair potential. The symbols indicate the following phases as detected by visual inspection of the MC configurations: ■: fluid; ●: gas+liquid; □: ZnS + gas; ▲: ZnS + liquid.

agreement with the phase regions predicted from the theoretical calculation, whereas at low ($q < 0.3$–0.4) or high ($q > 1.3$) values of q, a discrepancy of the simulation result from the theoretical prediction can be observed. We interpret this discrepancy as a result of the finite pressure considered in the computer simulations. Furthermore, the simulations are performed at a fixed value of the temperature, and the attraction strength, while the size ratio and the contact angle are varied. Such changes affect the effective droplet-colloid attraction strength, and thus the second virial coefficient, as shown by Noro and Frenkel [56] for short-ranged, isotropic potentials, and Foffi and Sciortino [57] for patchy potentials. As a result, the simulated points at small size ratios and contact angles correspond to lower effective droplet-colloid attraction [see Eqs. (2), (6), and (7)] or, equivalently, to higher temperatures. This may explain why the fluid phase is more stable at small size ratios and contact angles.

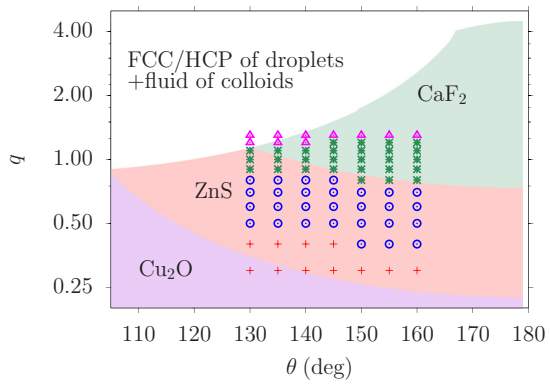

FIG. 7. Phase behavior of binary colloid-droplet mixtures determined by the theoretical prediction at infinite pressures (differently colored regions) and by computer simulation (differently shaped points): crosses indicate the homogeneous fluid phases (red), circles indicate ZnS phases (blue), asterisks indicate CaF_2 phases (green), and triangles represent fcc or hcp of droplets-fluid of colloids coexistence (pink). The vertical and horizontal axes indicate the size ratio q and contact angle θ between droplets and colloids, respectively.

IV. NONTETRAHEDRAL PATCH ARRANGEMENTS

We next discuss the results obtained by means of computer simulations for some particular cases of the patch arrangement. It is well known that the stable crystal structure of a binary atomic compound depends not only on the composition, concentration, and atomic size, but also on the coordination number (valence) as well as on the bond angles between atoms. A variety of questions arises naturally for crystals of corresponding colloid-droplet mixtures, e.g., how the crystal structure changes if the patch arrangement on the colloid surface changes or how the patch properties such as size, position, and strength of the attraction affect the resulting crystal structure. In principle, a variety of types of patch arrangements on the colloid surface is possible based on cluster configurations [39,58–60] and recent experimental

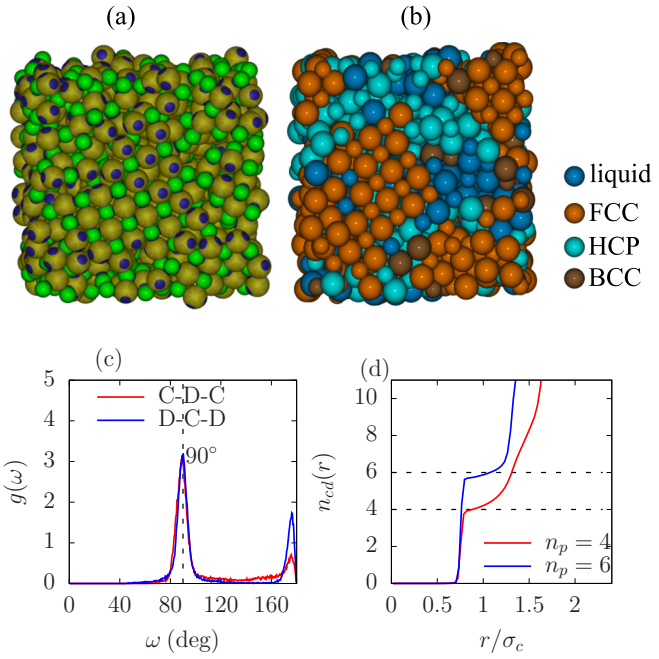

FIG. 8. (a),(b) Same as Figs. 3(a) and 3(b), respectively, but for patches that are arranged in square planer symmetry. The droplets (green spheres) are attached to the attractive patches (blue area part) of the colloids (yellow spheres) in a three-dimensional ordered structure. (c) Angular distribution functions for the colloid-droplet-colloid and droplet-colloid-droplet exhibit one strong peak at 90°, indicating right bond angles between two species. (d) The coordination number as a function of the scaled distance with different numbers of patches n_p: square planar ($n_p = 4$) and octahedral patch ($n_p = 6$) arrangement. The dashed lines indicate the coordination number of ideal crystal structures.

findings [8]. We first consider the case where patches are arranged in a square. In detail, each colloid has its four patches positioned at the corners of the square, which lie on a great circle of the spherical colloid surface. For a set of parameters, $q = 0.7$, $\theta = 140^\circ$, $\eta_c = 0.375$, $\eta_d = 0.128$, and $N_d/N_c = 1$, Figs. 8(a) and 8(b) show that the resulting equilibrium phase obtained from the simulations consists of two interpenetrating fcc or hcp lattices with the bond angle between colloids with droplets (and vice versa) equaling nearly 90° [Fig. 8(c)]. To the best of our knowledge, this crystal structure has no known atomic analog.

In octahedral patchy symmetry, each colloid has its six droplets arranged around a central colloid, defining the vertices of an octahedron. The resulting phase of the octahedral patchy colloid-droplet mixture is very similar to that of the planar square patchy colloid-droplet mixture, as described above, but with the important difference that the colloid-droplet coordination number equals six instead of four [see Fig. 8(d)]. Therefore, the octahedral patchy colloid-droplet mixture forms the NaCl/NiAs structure.

V. CONCLUSIONS

In summary, we studied a binary patchy colloid-droplet mixture by means of Metropolis MC simulations, in combination with the calculation of close-packing curves. The colloid-colloid and droplet-droplet pair interactions are taken to be purely hard-core potentials, while the colloid-droplet pair interaction has an attractive well that is parabolically dependent on distance in order to model the Pickering effect. This cross interaction is modulated by a Gaussian-like function to characterize a directional colloid-droplet pair interaction. Although the Gaussian-like potential is used as a generic model, its corresponding quantities can be controlled by the asymmetric wetting property of the colloid surface with the droplets, i.e., attractive parts are partial wetting, whereas the repulsive parts correspond to nonwetting or drying.

The analysis of the close-packing curves and total energy for a set of perfect structure proposals that possess regularly tetrahedral bond angles enables one to predict stable crystal structures at infinite pressures. The simulation results show the stability of the ZnS and CaF_2 structure, and fcc or hcp phase of large spheres with a dispersed fluid of small spheres, which is in good agreement with the theoretical predictions for a specific range of size ratios, i.e., $q = 0.4$–1.3. Discrepancies of theoretical predictions from simulations appear at low and high size ratios. More precisely, only the homogeneous fluid phase is observed at $q = 0.27$, instead of the Cu_2O phase as predicted by theory. In addition, fcc- or hcp-fluid phase coexistence can be observed in the simulation at $q = 1.5$, instead of the CaF_2 structure. Note also that although micro- or nanosized colloidal crystals of ZnS and CaF_2 are promising in photonic applications, they have not yet been synthesized in experiments. Therefore, our simulation results can be a useful guide to prepare these structures.

Furthermore, the (η_d, η_c)-phase diagram at $q = 0.75$ in the case of the anisotropic interaction exhibits a richer variety of phases compared to that of an isotropic interaction. We found that ZnS-gas and ZnS-fluid phase separations are possible.

Based on a unique configuration of colloidal clusters, we examined crystal structures for colloid-droplet mixtures in which the patches on the colloid surface are arranged in a well-defined polyhedron. As an example of octahedral patch symmetry, the NaCl/NiAs crystal structure can be observed. However, there is no atomic analog to the crystal structure of binary mixtures with patches arranged in square plane symmetry. These findings suggest that binary mixtures of patchy colloids and emulsion droplets could provide a different way to control the formation of increasingly complex colloidal crystal structures.

Future work could be directed towards developing and applying density functional theories [61,62] for colloid-droplet mixtures, possibly along the lines of of fundamental-measure theory [63,64], as derived for additive soft core mixtures [65] and binary nonadditive hard-sphere mixtures [66]. The patchy interactions could potentially be included along the lines of work of de las Heras and co-workers, who have convincingly shown that Wertheim theory is reliable in predicting the properties of patchy particle systems; see Refs. [26,67–70]. Having such a density functional theory (DFT) would allow one to study, e.g., capillary phase behavior [71].

ACKNOWLEDGMENTS

This work was funded by the Vietnamese National Foundation for Science and Technology Development (NAFOSTED) under Grant No. 103.02-2017.328.

APPENDIX A: BOND ORDER PARAMETERS

In order to characterize the local environment of a given particle i, Steinhardt *et al.* [72] proposed rotationally invariant bond order parameters, defined as

$$q_l(i) = \sqrt{\frac{4\pi}{2l+1}\sum_{m=-l}^{l}|q_{lm}(i)|^2}, \tag{A1}$$

where q_{lm} is the complex function given by

$$q_{lm}(i) = \begin{cases} 0 & \text{if } N_b(i) = 0 \\ \frac{1}{N_b(i)}\sum_{j=1}^{N_b(i)} Y_{lm}(\theta_{ij}, \varphi_{ij}) & \text{otherwise,} \end{cases} \tag{A2}$$

where $Y_{lm}(\theta_{ij}, \varphi_{ij})$ are spherical harmonics, and θ_{ij} and φ_{ij} are the polar and azimuthal angles of the relative vector $\mathbf{r}_{ij}$ between particle i and j with respect to an arbitrary reference frame. $N_b(i)$ is the number of the nearest neighbors of the particle i, l is an integer, and m is an integer which runs from $-l$ to l.

Recently, Lechner and Dellago [46] have introduced a modified version of the Steinhardt *et al.* order parameters in such a way that the additional information derived from the second nearest neighbors is taken into account, defining the so-called averaged bond order parameters,

$$\bar{q}_l(i) = \sqrt{\frac{4\pi}{2l+1}\sum_{m=-l}^{l}|\bar{q}_{lm}(i)|^2} \tag{A3}$$

TABLE II. Bond order parameters for different structures [74,75].

Geometry	$\bar{q}_4$	$\bar{q}_6$	$\bar{w}_4$	$\bar{w}_6$
fcc	0.19094	0.57452	−0.15932	−0.0136
hcp	0.09722	0.48476	0.13410	−0.01244
bcc	0.03637	0.51069	0.15932	0.01316
SC	0.76376	0.35355	0.15932	0.01316
Icosahedral	0	0.66332	0	−0.16975
Liquid	0	0	0	0

and

$$\bar{w}_l(i) = \frac{\sum_{m_1+m_2+m_3=0} \begin{pmatrix} l & l & l \\ m_1 & m_2 & m_3 \end{pmatrix} \bar{q}_{lm_1}(i)\bar{q}_{lm_2}(i)\bar{q}_{lm_3}(i)}{\left(\sum_{m=-l}^{l} |\bar{q}_{lm}(i)|\right)^{3/2}}, \tag{A4}$$

where the coefficient $\begin{pmatrix} l & l & l \\ m_1 & m_2 & m_3 \end{pmatrix}$ is the Wigner $3-j$ symbol [73]. The integers m_1, m_2, and m_3 run from $-l$ to l, but with the constraint $m_1+m_2+m_3=0$, and $\bar{q}_{lm}(i)$ is defined as

$$\bar{q}_{lm}(i) = \frac{1}{\widetilde{N}_b(i)} \sum_{k=0}^{\widetilde{N}_b(i)} q_{lm}(k). \tag{A5}$$

Here, the sum for k runs for all neighboring particles $\widetilde{N}_b(i)$ of particle i, plus the particle i itself. In our analysis, the neighbors of particle i are defined as those particles located within the distance cutoff corresponding to the first minimum of radial distribution functions. Using the averaged bond order parameters allows one to improve the accuracy of the distinction of different crystalline phases and clusters, i.e., fcc, hcp, and bcc. The crystalline structure around a given particle is sufficiently determined by the combination of three average local bond order parameters $\bar{q}_6$, $\bar{w}_4$, and $\bar{w}_6$. The values of bond order parameters for several perfect crystal structures are listed in Table II.

In order to classify the state of particles into liquidlike, fcc-like, hcp-like, and bcc-like, we use the following criteria [76]. First, if $\bar{q}_6 < 0.3$, the particle is classified as liquidlike. Otherwise, if $\bar{q}_6 > 0.3$, it is considered as crystalline. If the particle is crystalline and $\bar{w}_6 > 0$, it is classified as bcc-like. If the particle is not bcc-like but crystalline, $\bar{w}_4$ will be checked. If $\bar{w}_4 > 0$, the particle is hcp-like, and otherwise it is fcc-like (see Table III).

TABLE III. Criterion to determine the state of a particle based on average local bond order parameters [76].

State of a particle	$\bar{q}_6$	$\bar{w}_4$	$\bar{w}_6$
Liquid	$\bar{q}_6 < 0.3$		
bcc structure	$\bar{q}_6 > 0.3$		$\bar{w}_6 > 0$
hcp structure	$\bar{q}_6 > 0.3$	$\bar{w}_4 > 0$	$\bar{w}_6 < 0$
fcc structure	$\bar{q}_6 > 0.3$	$\bar{w}_4 < 0$	$\bar{w}_6 < 0$

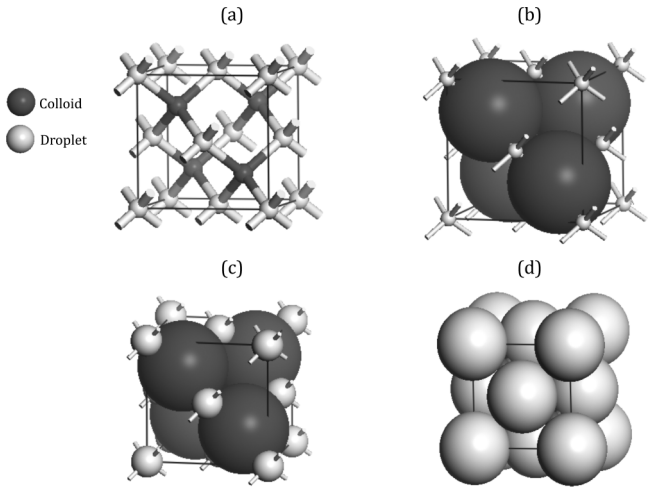

FIG. 9. Sketches of the structure and possible arrangements of zinc-blende structure. (a) Cubic unit cell containing four D (bright) spheres and four C (dark) spheres; the bond between the D and C spheres is indicated by a line connecting them together. (b) Arrangement with C-C (colloid-colloid) contact. (c) Arrangement with C-D (colloid-droplet) overlapping. (d) Arrangement with D-D (droplet-droplet) contact in the unit cell.

APPENDIX B: CLOSE-PACKING CALCULATIONS

In a regular tetrahedral structure, a central colloid has four droplets that are located at the corners of a tetrahedron such that the bond angles are ∼109.5°. From the crystallographic data for known atomic structure types [47], we find a small number of the crystal structures with D_nC_m stoichiometry that possess a regular tetrahedral bond distribution, including ZnS (zinc blende), ZnS (wurtzite), NaTl (zintl phase), CaF_2 (flourite), O_2Si (β − cristobalite), and Cu_2O (cuprite) structure type. We note that the constraint condition for the D-C-D (droplet-colloid-droplet) bond angle is ∼109.5°, whereas the C-D-C (colloid-droplet-colloid) bond angle is arbitrary. The packing fraction η as a function of size ratio $q = \sigma_d/\sigma_c$, with σ_d (σ_c) the diameter of droplets (colloids), which is known as the close-packing curve, usually has three branches corresponding to different contact regions between spherical particles. We discuss the close-packing curve for all structure types found in the following.

1. Zinc blende (ZnS)

The zinc-blende structure is named after the mineral zinc blende (sphalerite) in which the two types of spheres form two interpenetrating fcc lattices. The zinc-blende structure has two regular tetrahedral symmetries: each droplet is surrounded by four colloids and, conversely, each colloid is surrounded by four droplets, positioned at four vertices of the regular tetrahedron [see Fig. 9(a)]. We consider each branch of the close-packing curve separately in the following.

a. Colloid-colloid contact (C-C contact)

For small q, the positions of the droplet spheres are not uniquely defined and colloid-colloid contacts occur as shown in Fig. 9(b), and hence $a = 2\sqrt{2}r_c$, with a the cubic unit-cell

parameter. The packing fraction for this branch of the close-packing curve is given by

$$\eta = \frac{4 \times \frac{4}{3}\pi r_c^3 + 4 \times \frac{4}{3}\pi r_d^3}{a^3} = \frac{\pi(q^3+1)}{3\sqrt{2}}, \tag{B1}$$

where r_d and r_c are the radius of droplets and colloids, respectively. The factor 4 in front of the volume of the colloid and the droplet is the number of colloids and droplets in the unit cell.

As q increases, the droplet spheres touch and then, at a particular value of q, overlap with their nearest-neighbor colloid spheres [Fig. 9(b)]. The overlap distance is directly related to the contact angle θ, the droplet radius r_d, and the colloid radius r_c. When the overlap occurs, we have

$$a = 2\sqrt{2}r_c, \quad \frac{a\sqrt{3}}{4} = r_d + r_c - r_0, \tag{B2}$$

where $r_0 = r_d(1+\cos\theta)$. One obtains a bound for q ($q \leqslant q_1$) as

$$q_1 = \frac{1-\sqrt{3/2}}{\cos\theta}. \tag{B3}$$

b. Colloid-droplet overlap (C-D overlap)

For $q > q_1$, the colloidal spheres are no longer in contact with each other, but the droplets and colloidal spheres still overlap; thus,

$$\eta = \frac{4 \times \frac{4}{3}\pi r_c^3 + 4 \times \frac{4}{3}\pi r_d^3 - 16V_0}{a^3}, \tag{B4}$$

where V_0 is the volume of the intersection region formed by one colloid and one droplet sphere, given by

$$V_0 = \frac{\pi(r_d + r_c - B)^2\left(B^2 + 2Br_c + 2Br_d - 3r_c^2 - 3r_d^2 + 6r_cr_d\right)}{12B}, \tag{B5}$$

where B is the center-center distance between the droplet and the colloid at which the parabolic well has a minimum value (see the definition of the parabolic well in the main text). Multiplication by the factor of 16 in Eq. (B4) is due to the number of bonds between the colloids and droplets in the unit cell. Equation (B4) for the second branch of the close-packing curve becomes

$$\eta = \frac{\pi\sqrt{3}\{4 + q^3(3q-4) + q\cos\theta[4(q^3 - 3q^2 - 1) + q^2\cos\theta(6q + 4\cos\theta - q\cos^2\theta)]\}}{16(q\cos\theta - 1)^4}. \tag{B6}$$

As q is large enough, the droplet spheres can touch each other and the overlaps between the colloid and droplet spheres are still kept. We have the second bound q_2 ($q \leqslant q_2$) [see Fig. 9(c)],

$$\begin{aligned} a\sqrt{2} &= 4r_d, \\ \frac{a\sqrt{3}}{4} &= r_d + r_c - r_0, \end{aligned} \tag{B7}$$

i.e.,

$$q_2 = \frac{1}{\cos\theta + \sqrt{3/2}}. \tag{B8}$$

c. Droplet-droplet contact (D-D contact)

For $q > q_2$, the positions of the colloidal spheres become no longer unique and droplets are in contact with each other [Fig. 9(d)]. The packing fraction η is similar to that of the colloid-colloid contact, but $a = 2\sqrt{2}r_d$, and, therefore,

$$\eta = \frac{\pi\sqrt{2}}{6}\left(\frac{1+q^3}{q^3}\right). \tag{B9}$$

2. Wurtzite (ZnS)

The wurtzite and zinc-blende structure belong to a set of homeotect structure types; i.e., every D sphere has the same number of nearest D neighbors and the same number of nearest C neighbors, and, conversely, every C sphere has the same number of nearest D neighbors and C neighbor atoms. Therefore, the wurtzite and zinc-blende structure have the same close-packing curve [48,49].

Similarly, we calculate the close-packing curve for the other crystal structures. The results are given below.

3. Zintl phase (NaTl)

The compound NaTl is a classical example of a zintl phase whose thallium (C) partial structure is the diamond lattice. However, different from all structures listed, the close-packing curve for the NaTl structure has only two branches, i.e., one for C-C contact and the other for D-D contact. This means that C-D overlap is impossible, and hence the NaTl structure cannot be a candidate for stable structures based on the Pickering mechanism.

a. Colloid-colloid contact (C-C contact)

The packing fraction for this branch of the close-packing curve is given by

$$\eta = \frac{\pi\sqrt{3}}{16}(1+q^3), \tag{B10}$$

with $0 \leqslant q \leqslant 1$.

b. Droplet-droplet contact (D-D contact)

$$\eta = \frac{\pi\sqrt{3}}{16}\left(\frac{1+q^3}{q^3}\right), \tag{B11}$$

with $q \geqslant 1$.

4. Flourite (CaF_2)

a. Colloid-colloid contact (C-C contact)

$$\eta = \frac{\pi}{12}(2 + q^3), \tag{B12}$$

with $0 \leqslant q \leqslant \frac{1-\sqrt{3}}{\cos\theta}$.

b. Colloid-droplet overlap (C-D overlap)

$$\eta = \frac{\pi\sqrt{3}[32 - 48q^3 + 45q^4 + 8q\cos\theta(6q^3 - 9q^2 - 4) + q^3(20q\cos 2\theta + 8\cos 3\theta - q\cos 4\theta)]}{64(q\cos\theta - 1)^4}, \tag{B13}$$

with $\frac{1-\sqrt{3}}{\cos\theta} < q \leqslant \frac{1}{\cos\theta+\sqrt{3/2}}$.

c. Droplet-droplet contact (D-D contact)

$$\eta = \frac{\pi\sqrt{2}}{6}\left(\frac{1 + q^3}{q^3}\right), \tag{B14}$$

with $q > \frac{1}{\cos\theta+\sqrt{3/2}}$.

5. $\beta -$ cristobalite(O_2Si)

a. Colloid-colloid contact (C-C contact)

If there is only C-C contact, then the D diameter must be zero. Hence, $q = 0$ and $\eta = 0.34$ as C spheres are located at the positions of the diamond lattice.

b. Colloid-droplet overlap (C-D overlap)

$$\eta = \frac{\pi\sqrt{3}\{4 + 3q^4 - q\cos\theta[4 + 12q^2 + q^2\cos\theta(q\cos^2\theta - 4\cos\theta - 6q)]\}}{64(q\cos\theta - 1)^4}, \tag{B15}$$

with $0 < q \leqslant \frac{1}{\cos\theta+\sqrt{3/2}}$.

c. Droplet-droplet contact (D-D contact)

$$\eta = \frac{\pi}{12\sqrt{2}}\frac{1 + 2q^3}{q^3}, \tag{B16}$$

with $q > \frac{1}{\cos\theta+\sqrt{3/2}}$.

6. Cuprite (Cu_2O)

a. Colloid-colloid contact (C-C contact)

Similarly to the $\beta -$ cristobalite structure, only C-C contact occurs if the D diameter is zero, and hence $\eta = 0.68$ as C spheres are located at body-center-cubic positions.

b. Colloid-droplet overlap (C-D overlap)

$$\eta = \frac{\pi\sqrt{3}\{4 + 3q^4 - q\cos\theta[4 + 12q^2 + q^2\cos\theta(q\cos^2\theta - 4\cos\theta - 6q)]\}}{32(q\cos\theta - 1)^4}, \tag{B17}$$

with $0 < q \leqslant \frac{1}{\cos\theta+\sqrt{3/2}}$.

c. Droplet-droplet contact (D-D contact)

$$\eta = \frac{\pi}{6\sqrt{2}}\frac{(1 + 2q^3)}{q^3}, \tag{B18}$$

with $q > \frac{1}{\cos\theta+\sqrt{3/2}}$.

[1] Special Issue on "Designed Colloidal Self-Assembly," edited by A. V. Petukhov and G. J. Vroege (MDPI publishing, Basel, 2017).
[2] J. H. Holtz and S. A. Asher, Nature (London) **389**, 829 (1997).
[3] P. Jiang, J. Cizeron, J. F. Bertone, and V. L. Colvin, J. Am. Chem. Soc. **121**, 7957 (1999).
[4] J. D. Joannopoulos, P. R. Villeneuve, and S. Fan, Nature (London) **386**, 143 (1997).
[5] Y. A. Vlasov, X.-Z. Bo, J. C. Sturm, and D. J. Norris, Nature (London) **414**, 289 (2001).
[6] K. M. Ho, C. T. Chan, and C. M. Soukoulis, Phys. Rev. Lett. **65**, 3152 (1990).
[7] M. Maldovan and E. L. Thomas, Nat. Mater. **3**, 593 (2004).
[8] Y. Wang, Y. Wang, D. R. Breed, V. N. Manoharan, L. Feng, A. D. Hollingsworth, M. Weck, and D. J. Pine, Nature (London) **491**, 51 (2012).
[9] G.-R. Yi, D. J. Pine, and S. Sacanna, J. Phys. Condens. Matter **25**, 193101 (2013).
[10] E. Bianchi, R. Blaak, and C. N. Likos, Phys. Chem. Chem. Phys. **13**, 6397 (2011).
[11] Q. Chen, S. C. Bae, and S. Granick, Nature (London) **469**, 381 (2011).
[12] X. Mao, Q. Chen, and S. Granick, Nat. Mater. **12**, 217 (2013).
[13] A. B. Pawar and I. Kretzschmar, Macromol. Rapid Commun. **31**, 150 (2010).
[14] D. J. Kraft, J. Groenewold, and W. K. Kegel, Soft Matter **5**, 3823 (2009).
[15] A. V. Tkachenko, Phys. Rev. Lett. **89**, 148303 (2002).
[16] Zhang, A. S. Keys, T. Chen, and S. C. Glotzer, Langmuir **21**, 11547 (2005).
[17] E. Bianchi, P. Tartaglia, E. Zaccarelli, and F. Sciortino, J. Chem. Phys. **128**, 144504 (2008).
[18] F. Romano, E. Sanz, and F. Sciortino, J. Phys. Chem. B **113**, 15133 (2009).
[19] F. Romano, E. Sanz, and F. Sciortino, J. Phys. Chem. **132**, 184501 (2010).
[20] F. Romano, E. Sanz, and F. Sciortino, J. Phys. Chem. **134**, 174502 (2011).
[21] E. Bianchi, G. Doppelbauer, L. Filion, M. Dijkstra, and G. Kahl, J. Phys. Chem. **136**, 214102 (2012).
[22] G. Doppelbauer, E. G. Noya, E. Bianchi, and G. Kahl, J. Phys.: Condens. Matter **24**, 284124 (2012).
[23] F. Smallenburg and F. Sciortino, Nat. Phys. **9**, 554 (2013).
[24] J. P. K. Doye, A. A. Louis, I.-C. Lin, L. R. Allen, E. G. Noya, A. W. Wilber, H. C. Kok, and R. Lyus, Phys. Chem. Chem. Phys. **9**, 2197 (2007).
[25] A.-P. Hynninen, J. H. J. Thijssen, E. C. M. Vermolen, M. Dijkstra, and A. van Blaaderen, Nat. Mater. **6**, 202 (2007).
[26] D. de las Heras, J. M. Tavares, and M. M. Telo da Gama, Soft Matter **7**, 5615 (2011).
[27] F. Seiferling, D. de las Heras, and M. M. T. da Gama, J. Chem. Phys. **145**, 074903 (2016).
[28] A. R. Denton and N. W. Ashcroft, Phys. Rev. A **42**, 7312 (1990).
[29] M. J. Murray and J. V. Sanders, Philos. Mag. A **42**, 721 (1980).
[30] S. Hachisu and S. Yoshimura, Nature (London) **283**, 188 (1980).
[31] M. Hasaka, H. Nakashima, and K. Oki, Trans. Jpn. Inst. Met. **25**, 65 (1984).
[32] L. Filion and M. Dijkstra, Phys. Rev. E **79**, 046714 (2009).
[33] A. B. Hopkins, Y. Jiao, F. H. Stillinger, and S. Torquato, Phys. Rev. Lett. **107**, 125501 (2011).
[34] A. B. Hopkins, F. H. Stillinger, and S. Torquato, Phys. Rev. E **85**, 021130 (2012).
[35] X. Cottin and P. A. Monson, J. Chem. Phys. **102**, 3354 (1995).
[36] M. Maldovan, C. K. Ullal, W. C. Carter, and E. L. Thomas, Nat. Mater. **2**, 664 (2003).
[37] A. Fortini, Phys. Rev. E **85**, 040401(R) (2012).
[38] F. L. Román, M. Schmidt, and H. Löwen, Phys. Rev. E **61**, 5445 (2000).
[39] I. Schwarz, A. Fortini, C. S. Wagner, A. Wittemann, and M. Schmidt, J. Chem. Phys. **135**, 244501 (2011).
[40] H. Pham Van, A. Fortini, and M. Schmidt, Phys. Rev. E **93**, 052609 (2016).
[41] H. Pham Van, A. Fortini, and M. Schmidt, Materials **10**, 361 (2017).
[42] P. Pieranski, Phys. Rev. Lett. **45**, 569 (1980).
[43] E. G. Noya, C. Vega, J. P. K. Doye, and A. A. Louis, J. Chem. Phys. **132**, 234511 (2010).
[44] J. Liu and E. Luijten, Phys. Rev. Lett. **92**, 035504 (2004).
[45] S. Whitelam and P. L. Geissler, J. Chem. Phys. **127**, 154101 (2007).
[46] W. Lechner and C. Dellago, J. Chem. Phys. **129**, 114707 (2008).
[47] P. Villars, K. Mathis, and F. Hulliger, in *The Structures of Binary Compounds*, edited by F. R de Boer and D. G. Pettifor (North-Holland, Amsterdam, 1989).
[48] E. Parthé, Z. Kristallogr. Cryst. Mater. **115**, 52 (1961).
[49] E. Parthé, *Crystal Chemistry of Tetrahedral Structures* (Gordon and Breach, PA, 1964).
[50] M. Dijkstra, R. van Roij, and R. Evans, Phys. Rev. E **59**, 5744 (1999).
[51] N. A. Mahynski, A. Z. Panagiotopoulos, D. Meng, and S. K. Kumar, Nat. Commun. **5**, 4472 (2014).
[52] N. A. Mahynski, S. K. Kumar, and A. Z. Panagiotopoulos, Soft Matter **11**, 5146 (2015).
[53] N. A. Mahynski, S. K. Kumar, and A. Z. Panagiotopoulos, Soft Matter **11**, 280 (2015).
[54] N. A. Mahynski, L. Rovigatti, C. N. Likos, and A. Z. Panagiotopoulos, ACS Nano **10**, 5459 (2016).
[55] F. Romano and F. Sciortino, Nat. Commun. **3**, 975 (2012).
[56] M. G. Noro and D. Frenkel, J. Chem. Phys. **113**, 2941 (2000).
[57] G. Foffi and F. Sciortino, J. Phys. Chem. B **111**, 9702 (2007).
[58] V. N. Manoharan, M. T. Elsesser, and D. J. Pine, Science **301**, 483 (2003).
[59] Y. S. Cho, G. R. Yi, Y. S. Chung, S. B. Park, and S. M. Yang, Langmuir **23**, 12079 (2007).
[60] C. Wagner, B. Fischer, M. May, and A. Wittemann, Colloid. Polym. Sci. **288**, 487 (2010).
[61] R. Evans, Adv. Phys. **28**, 143 (1979).
[62] R. Evans, M. Oettel, R. Roth, and G. Kahl, J. Phys. Condens. Matter **28**, 240401 (2016).
[63] R. Roth, J. Phys. Condens. Matter **22**, 063102 (2010).
[64] P. Tarazona, J. Cuesta, and Y. Martínez-Ratón, *Density Functional Theories of Hard Particle Systems* (Springer, Berlin, 2008), pp. 247–341.
[65] M. Schmidt, Phys. Rev. E **62**, 3799 (2000).
[66] M. Schmidt, J. Phys. Condens. Matter **16**, L351 (2004).
[67] D. de las Heras, J. M. Tavares, and M. M. T. da Gama, J. Chem. Phys. **134**, 104904 (2011).

[68] N. Gnan, D. de las Heras, J. M. Tavares, M. M. T. da Gama, and F. Sciortino, J. Chem. Phys. **137**, 084704 (2012).
[69] D. de las Heras, J. M. Tavares, and M. M. Telo da Gama, Soft Matter **8**, 1785 (2012).
[70] L. Rovigatti, D. de las Heras, J. M. Tavares, M. M. T. da Gama, and F. Sciortino, J. Chem. Phys. **138**, 164904 (2013).
[71] A. Fortini, M. Schmidt, and M. Dijkstra, Phys. Rev. E **73**, 051502 (2006).
[72] P. J. Steinhardt, D. R. Nelson, and M. Ronchetti, Phys. Rev. B **28**, 784 (1983).
[73] A. Messiah, *Quantum Mechanics* (North-Holland, Amsterdam, 1965).
[74] J. S. van Duijneveldt and D. Frenkel, J. Chem. Phys. **96**, 4655 (1992).
[75] S. Winczewski, J. Dziedzic, and J. Rybicki, Comput. Phys. Commun. **198**, 128 (2016).
[76] J. P. Mithen and R. P. Sear, Cryst. Growth Des. **16**, 3049 (2016).